文章编号: 1001-9014(2018)06-0668-05　　DOI:10.11972/j.issn.1001-9014.2018.06.005

2D-carrier profiling in narrow quantum wells by a Schottky's current transport model based on scanning spreading resistance microscopy

HUANG Wen-Chao[1], WANG Xiao-Fang[2*], CHEN Xiao-Shuang[2], XUE Yu-Xiong[1*], YANG Sheng-Sheng[1]

(1. National Laboratory for Vacuum Technology and Physics, Lanzhou Institute of Physics, Lanzhou 730000, China;
2. National Laboratory for Infrared Physics, Shanghai Institute of Technical Physics,
Chinese Academy of Sciences, Shanghai 200083, China)

Abstract: Current studies on the relationship between carrier concentration in nano-scale semiconductor structure and its local conductance is mainly on parameters fitting. For above connection, existing models rely on artificial fitting parameters such as ideal factor. For above reason, derivation of carrier concentration though measured local conductance can not be done. In this work, we present a scheme to obtain the carrier concentration in narrow quantum wells (QWs). Cross-sectional scanning spreading resistance microscopy (SSRM) provides unparalleled spatial resolution (<10 nm, Capable of characterizing single QW layer) in electrical characterization. High-resolution local conductance has been measured by SSRM on molecular beam epitaxy-grown GaAs/AlGaAs QWs cleaved surface (110). Based on our experimental set-up, a model which describes conductance by the only argument, i. e. carrier concentration has been built. Using the model, our implementation derived carrier concentration from SSRM measured local conductance in GaAs/AlGaAs QWs (doping level: $10^{16}/cm^3 - 10^{18}/cm^3$). Relative errors of the results are within 30%.

Key words: carrier concentration, quantum wells, scanning spreading resistance microscopy, Schottky
PACS: 73.25.+i, 73.40.Cg, 07.05.Tp, 73.61.Ey

基于肖特基电流输运模型和扫描分布电阻显微术的窄量子阱载流子浓度表征

黄文超[1], 王晓芳[2*], 陈效双[2], 薛玉雄[1*], 杨生胜[1]

(1. 兰州空间技术物理研究所 真空技术与物理国家重点实验室,甘肃 兰州　730000;
2. 中国科学院上海技术物理研究所 红外物理国家重点实验室,上海　200083)

摘要:目前对于纳米尺度半导体材料的局域电导与对应载流子浓度关系的描述主要以参数拟合为主。其关系模型主要依赖人工拟合参数,例如理想因子。所以无法从测得局域电导分布来推出载流子浓度分布。为此,提出了一种获取量子阱中载流子浓度的模型。通过小于10 nm分辨的截面扫描分布电阻显微术,测得了GaAs/AlGaAs量子阱(1 1 0)截面的局域电导分布。基于实验设置,提出了只含有掺杂浓度参量的实验描述模型。通过模型,由测得的量子阱(掺杂浓度从 $10^{16}/cm^3$ 到 $10^{18}/cm^3$)局域电导分布,推导出了其载流子分布。相对误差在30%之内。

关　键　词:载流子浓度;量子阱;扫描分布电阻显微术;肖特基

中图分类号:O469　　**文献标识码**:A

Received date: 2018-03-21, **revised date**: 2018-08-24　　**收稿日期**:2018-03-21, **修回日期**:2018-08-24

Foundation items: Supported by China Aerospace Science and Technology Corporation Research and Development Innovation Project (YJT0410), the Fund of Shanghai Science and Technology Foundation (16ZR1447400), the National Key Research and Development Program of China (2016YFB0501303)

Biography: HUANG Wen-Chao(1985-), male, Lanzhou, China, Ph. D. Research area focus on semiconductor physics. E-mail: huangwcnk@163.com

* **Corresponding author**: E-mail: wxiaof66@mail.sitp.ac.cn, cheng20050322@163.com

Introduction

The electric and opto-electronic function of semiconductor devices is normally realized by controllable doping in well-designed band structures, thus the actual carrier distribution is among those explicit information for space radiation failure analysis as well as performance prediction. Particularly, for quantum wells (QWs) devices, which have been widely adopted for light emission and detection[1-6]. The carrier concentration has a direct impact on their efficiency and leakage property. In recent years, scanning spreading resistance microscopy (SSRM), which can be used to carry out electrical characterization in nanometer scale, has emerged as a promising tool to profile the doping property in functional materials[7]. However, there are few SSRM studies on QWs structures. At the same time, derivation carrier concentration form SSRM measured local conductance is imperative but has not been well realized.

Conventionally, to get reliable spreading resistance, relatively large force (μN) is applied to keep a stable tip-sample contact[8-10]. For the highly doped area, this leads to an ohmic contact between the metallic tip and semiconductor that can be described by thermionic field emission (TFE)[11]. However, for those moderate or lowly doped ones, which form a typical Schottky contact with tips, TFE mode is no longer suitable. So far fitting parameters are commonly introduced in order to reproduce the experimental results[12-15]. Therefore, derivation carrier concentration form detected SSRM local conductance has not yet been well realized.

Here, we present a scheme to get the carrier concentration in narrow QWs based on SSRM measurement. The experimental parameters are delicately selected to maintain Schottky contact between tip and QWs. Thermionic emission (TE) is adopted as current transport mechanism. The influence of carrier concentration is represented as Schottky barrier lowering through TFE and image force (IMF) effects. Our scheme is demonstrated to be capable of obtaining carrier concentration in GaAs/AlGaAs QWs with doping level from 10^{16} cm^{-3} to 10^{18} cm^{-3}.

1 Experiment

Epitaxial GaAs/AlGaAs QWs (n-type doping) were grown on GaAs (001) substrate by molecular beam epitaxy (MBE) shown in Fig. 1. Carrier concentration of each well varies in a wide range, i. e. n_1 (5×10^{16} cm^{-3}), n_2 (1×10^{17} cm^{-3}), n_3 (5×10^{17} cm^{-3}) and n_4 (1.5×10^{18} cm^{-3}), which covers the doping level for most QWs based devices. All wells widths are 6nm. As shown in Fig. 1, there are n-type doping GaAs electrode layers with carrier concentration of 5×10^{17} cm^{-3}. For this QWs, electron effective mass is $0.063\ m_0$ (m_0 is electron rest mass), relative dielectric constant is 12.9 and effective density of states in conduction band is 4.3×10^{17} cm^{-3}.

Basic principle of the experiment is to keep a Schottky contact between SSRM tip and QWs during measuring

electrode layer	300 nm n-GaAs	5E175 cm^{-3}
	50 nm -$Al_{0.4}Ga_{0.6}As$	
n_4	6 nm n-GaAs	
	50 nm -$Al_{0.4}Ga_{0.6}As$	
n_3	6 nm n-GaAs	
	50 nm -$Al_{0.4}Ga_{0.6}As$	
n_2	6 nm n-GaAs	
	50 nm -$Al_{0.4}Ga_{0.6}As$	
n_1	6 nm n-GaAs	
	50 nm -$Al_{0.4}Ga_{0.6}As$	
electrode layer	50 nm n-GaAs	5E175 cm^{-3}

Fig. 1 N-type doping GaAs/AlGaAs QWs
图 1 N 型掺杂的 GaAs/AlGaAs 量子阱

process. Therefore, the force applied between tip and sample must remain small (dozens of nN), and the sample bias value should be set to less than 80% of the Schottky barrier height (SBH). SBH can be initially, crudely estimated by the work function difference between SSRM tip and QWs. In this case, the bias voltage through tip on QWs is set to 0.9 V. Under such circumstances, to get stable and reliable detection signal, sample roughness must be in angstrom level and a sharp tip with larger hardness than sample is demanded.

For cross-sectional SSRM characterization, a common electrode to connect all QWs must be made. Then, we cleave the sample along (110) crystal orientation to meet the sample roughness requirements of SSRM, which must be in angstrom dimension. The measurement range covers a wide value, from 10^5 Ω to 10^{11} Ω.

After all the above preparation, SSRM measurement can carry out on GaAs/AlGaAs QWs. Local conductance distribution for each quantum well is shown in Fig. 2. The ultimate limit of resolution in measurement is 10^{-12} A/V. The local conductance peak and FWHM (full width at half maximum) for each well is also shown in Table 1.

Table 1 Local conductance peak and FWHM for each well
表 1 每个量子阱的局域电导峰值与半峰宽数值

Quantum well	Local conductance peak/ (A/V)	FWHM/nm
n_1	7.87×10^{-11}	11.0
n_2	1.77×10^{-10}	10.0
n_3	9.84×10^{-10}	10.0
n_4	3.23×10^{-9}	10.6

2 The model and derivation of carrier concentration

SSRM tip and GaAs/AlGaAs QWs form a Schottky contact [16-17]. Current transport mechanism between tip and semiconducting QWs is called thermionic emission (TE) [18-19]. As for highly doped, i. e. degenerate semiconductors at low temperature, the current comes from

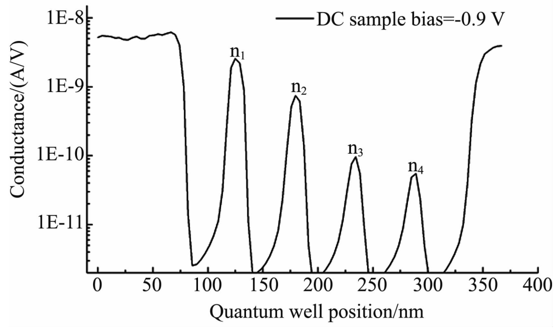

Fig. 2　High resolution local conductance measured by SSRM on GaAs/AlGaAs QWs with measurement limit of 10^{-12} A/V

图 2　GaAs/AlGaAs 量子阱的高分辨率局域电导测量，测量极限为 10^{-12} A/V

the tunneling of electrons with energies close to the Fermi level in the semiconductors. This is called thermionic field emission (TFE)[20-25]. However, using TFE as current transport mechanism in model, the results of derivation carrier concentration for degenerate semiconductors deviate heavily from real results. In fact, (i) Experiment temperature is relatively high, and most electrons have enough energy to go over the top of the barrier. The effect of tunneling is not predominant and the current transport characteristic is more like TE[26]. (ii) Tunneling of electrons is a quantization process. It is easy to be affected by many factors. Impurities in semiconductors and passivation cleaved surface have effect on the tunneling process. (iii) In our experiment, SSRM tip and QWs maintain a Schottky contact when the QWs are highly doped. TFE is more often used to describe an ohmic contact. In this case, for those highly doped semiconductors, we try to use TE as Schottky current transport mechanism but take TFE as an Schottky barrier lowering mechanism. Besides, image force (IMF)[27] is also considered as an SBH lowering mechanism. Then, the results of derivation carrier concentration for non-degenerate and degenerate semiconductors are both in good agreement with real results, which we will show later. Current density function for Schottky contact is shown in Eq. 1.

$$J_{\mathrm{TE}} = A^* T^2 \exp\left(\frac{q(\Phi_{\mathrm{Bn0}} - \Delta\Phi_{\mathrm{IMF}} - \Delta\Phi_{\mathrm{TFE}})}{kT}\right)\left(\exp\left(\frac{qV_F}{kT}\right) - 1\right) \quad , \quad (1)$$

$$A^* = \frac{4\pi q m^* k^2}{h^3} \quad , \quad (2)$$

where Φ_{Bn0} is the SBH between SSRM tip and QWs, $\Delta\Phi_{\mathrm{IMF}}$ is the decrease of SBH due to image force, $\Delta\Phi_{\mathrm{TFE}}$ is the decrease of SBH due to thermionic field emission, T is experimental temperature, q is unit charge, k is Boltzmann constant and V_{F} is forward bias. A^* is the effective Richardson constant shown in Eq. 2, where m^* is electron effective mass and h is Planck constant.

The two dominant SBH lowering mechanism $\Delta\Phi_{\mathrm{IMF}}$ and $\Delta\Phi_{\mathrm{TFE}}$ are shown in Eqs. 3-4 respectively.

$$\Delta\Phi_{\mathrm{IMF}} = \left[\frac{q^3 N |\Phi_{\mathrm{Bn0}} - \Phi_n - V_{\mathrm{F}}|}{8\pi^2 \varepsilon_s^3}\right]^{1/4} \quad , \quad (3)$$

$$\Delta\Phi_{\mathrm{TFE}} = \left(\frac{3}{2}\right)^{2/3} |\Phi_{\mathrm{Bn0}} - \Phi_n - V_{\mathrm{F}}|^{1/3} \quad , \quad (4)$$

$$E_{00} = \frac{qh}{4\pi}\sqrt{\frac{N}{m^* \varepsilon_s}} \quad , \quad (5)$$

where ε_{s} is relative dielectric constant of semiconductor, N is carrier concentration of semiconductors and Φ_{n} is the energy level difference between conduction band minimum and Fermi energy level of semiconductors. If we consider that local conductance peak is σ, current density is J_{TE} and the maximum contact area of SSRM tip-quantum wells is S, we have Eq. 6 below.

$$\sigma = \frac{J_{\mathrm{TE}} \times S}{V_{\mathrm{F}}} \quad . \quad (6)$$

In Fig. 3, circles represent the contact area of SSRM tip-quantum wells and barriers, and R represents the radius. d is the width of quantum well. On the left side of Fig. 3, the contact area of SSRM tip-quantum wells reaches the maximum, S in Eq. 7, which corresponds to the local conductance peak. On the right side of Fig. 3, the SSRM tip travels a distance of k and local conductance reaches half of its peak. Here, the contact area of SSRM tip-quantum wells Sh in Eq. 8, is half of its maximum S, which corresponds to the FWHM of local conductance. Via $S = 2Sh$, we can get R, i. e. S in Eq. 6.

$$S = 2R^2 \arcsin\left(\frac{d}{2R}\right) + d\sqrt{R^2 - \frac{d^2}{4}} \quad , \quad (7)$$

$$Sh = R^2 \arccos\left(\frac{k - \frac{d}{2}}{R}\right) - \left(k - \frac{d}{2}\right)\sqrt{R^2 - \left(k - \frac{d}{2}\right)^2} \quad . \quad (8)$$

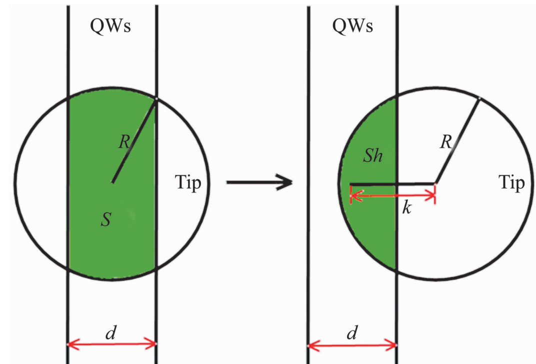

Fig. 3　Illustration shows the contact situation between SSRM tip and QWs. On the left, contact area of SSRM tip and quantum wells reaches maximum, and local conductance reaches maximum as well. On the right, contact area of SSRM tip and quantum wells is half of its maximum, and local conductance is half of its peak.

图 3　测量探针与量子阱接触示意图。左图为 SSRM 探针和量子阱的接触面积达到最大值的情况，此时测得局域电导也达到最大值。右图为 SSRM 测量探针与量子阱接触面积为最大值的一半，此时测得局域电导为峰值的一半

As we mentioned before, initial value of SBH can

be estimated by the work function difference between SSRM tip and QWs. However, the real SBH value should be derived for our model. Firstly, a current-voltage curve can be measured on same kind of material (GaAs in this case) with known carrier concentration. Then, SBH can be derived by fitting the current-voltage curve by equation. given in Eq. 1. Via Eqs. 1-2, a model relating QWs carrier concentration and local conductance is built. A carrier concentration-local conductance curve can be calculated by the model. Finally, with the measured local conductance of QWs, the carrier concentration of QWs can be derived through the curve.

To optimize our model, calculation will be complex and huge. Therefore, the above equations were compiled in C++ language so that modules in program would be tuned and recombined easily.

SSRM measurement on local conductance of GaAs/AlGaAs QWs has been performed in Sect. 1. Local conductance peak and FWHM for quantum wells n_1, n_2, n_3 and n_4 are listed in Table 1. As we discussed in Eq. (8), FWHM $=2k$. All quantum well widths are 6 nm. By means of Eq. 7, Eq. 8 and $S=2Sh$, we calculated that R almost maintains at 6.6 nm, although $2k$ changes from 10.0 nm to 11.0 nm. Then, $S=8.22\times10^{-17}$ m^2. The SBH between SSRM diamond coated tip and QWs is derived to be $\Phi_{Bn0}=1.178$ eV, by current-voltage relationship measuring and fitting on n-type doping GaAs electrode layers with carrier concentration of 5×10^{17} cm^{-3}.

With above equations and parameters compiled in C++ language, a carrier concentration-local conductance relationship curve is calculated, shown in Fig. 4. For comparison, we calculate the relationship curve by the TFE model as well. The curve calculated by TFE model has a typical ohmic contact character, while curve by our model reflects a Schottky behavior[11].

Based on the SSRM measured local conductance peak of each quantum well, carrier concentration for each well is determined through the curve calculated by our model, which is shown in Table 2. Relative error of the result is less than 30%. Results from the curve calculated by TFE model are also shown in Table 2 and relative errors are very large. With the optimizing on both experiment and our model, the relative error can be further decreased.

3 Summary

We introduced a novel methodology to obtain the carrier concentration in narrow QWs. Base on existing studies of parameter fitting between carrier concentration and measured local conductance for thin films, we built a

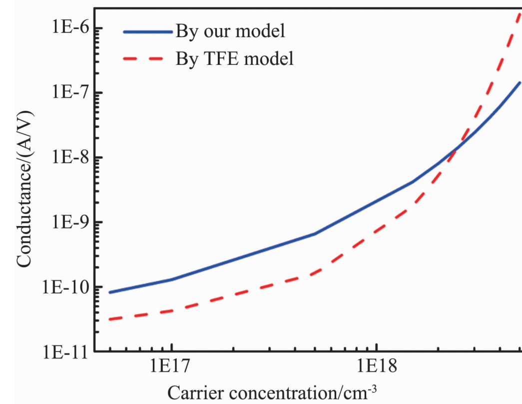

Fig. 4 Calculated relationship curve between carrier concentration and local conductance on GaAs/AlGaAs QWs mentioned in Sect. 1. Blue solid line represents that curve is calculated by our model and red dash line represents that curve is calculated by the TFE model

图4 第1节中提到的载流子浓度与局域电导之间的关系曲线。蓝色实线代表本研究的模型模拟出的结果,而红色虚线代表由TFE模型得出的结果

model in view of the actual current transport mechanism of Schottky contact. With all experimental parameters and theoretical formulae programmed in C++ language, the model has been optimized. Through the carrier concentration-local conductance curve calculated by the model, carrier concentration in each GaAs/AlGaAs quantum well can be derived via SSRM measured local conductance.

This scheme provides a universal carrier concentration detection method for narrow QWs with the width in nanometers. In particular, for semiconductor quantum well with narrow gap, unintentionally doped QWs, indirect doping in barriers QWs and coupled quantum well (CQW), this high-resolution and nondestructive scheme has a great advantage. Cross-sectional SSRM measurement is unaffected by other functional areas, therefore, this scheme is suitable for carrier concentration detection in selected quantum well layer of QWs with complex material structures. The scheme is non-consumptive, detection can be repeatable and the scheme is non- destructive.

References

[1] Xia H, Lu Z Y, Li T X, *et al*. Distinct photocurrent response of individual GaAs nanowires induced by n-type doping[J]. *Acs Nano*, 2012, **6**(7):6005-6013.

[2] Nakamura S, Senoh M, Iwasa N, *et al*. High-power InGaN single-

Table 2 Carrier concentration determined by our model and TFE model for each well

表2 本研究模型与TFE模型得出的每个量子阱载流子浓度数值

QWs number	Real carrier concentration /cm^{-3}	Carrier concentration by our model /cm^{-3}	Relative error of our model	Carrier concentration by TFE /cm^{-3}	Relative error of TFE
n_1	5E16	4.86E16	2.80%	2.86E17	472%
n_2	1E17	1.24E17	24.00%	5.47E17	447%
n_3	5E17	6.43E17	28.60%	1.26E18	152%
n_4	1.5E18	1.37E18	8.67%	2.49E18	66%

quantum-well-structure blue and violet light-emitting diodes[J]. *Appl. Phys. Lett.*, 1995, **67**(13):1868-1870.

[3] Choquette K D, Klem J F, Fischer A J, *et al.* Room temperature continuous wave InGaAsN quantum well vertical-cavity lasers emitting at 1.3 μm[J]. *Electron. Lett.*, 2000, **36**(16):1388-1390.

[4] Nakada N, Nakaji M, Ishikawa H, *et al.* Improved characteristics of InGaN multiple-quantum-well light-emitting diode by GaN/AlGaN distributed Bragg reflector grown on sapphire[J]. *Appl. Phys. Lett.*, 2000, **76**(14):1804-1806.

[5] Faist J, Capasso F, Sivco D L, *et al.* Quantum cascade laser[J]. *Science*, 1994, **264**:553-556.

[6] Williams B S, Callebaut H, Kumar S, *et al.* 3.4-THz quantum cascade laser based on longitudinal-optical-phonon scattering for depopulation[J]. *Appl. Phys. Lett.*, 2003, **82**(7):1015-1017.

[7] Shafai C, Thomson D J, Normandin M S, *et al.* Delineation of semiconductor doping by scanning resistance microscopy[J]. *Appl. Phys. Lett.*, 1994, **64**(3):342-344.

[8] Lu R P, Kavanagh K L, Dixon-Warren St J, *et al.* Calibrated scanning spreading resistance microscopy profiling of carriers in III-V structures[J]. *J. Vac. Sci. Technol. B*, 2001, **19**(4):1662-1670.

[9] Lu R P, Kavanagh K L, Dixon-Warren St J, *et al.* Scanning spreading resistance microscopy current transport studies on doped III - V semiconductors[J]. *J. Vac. Sci. Technol. B*, 2002, **20**(4):1682-1689.

[10] Hudait M K, Krupanidhi S B. Doping dependence of the barrier height and ideality factor of Au/n-GaAs Schottky diodes at low temperatures [J]. *Physica B*, 2001, **307**(1):125-137.

[11] Sze S M. *Physics of semiconductor devices*[M]. Second Edition, SuZhou, Suzhou University Press, 2003, 543.

[12] Lin Y J. Application of the thermionic field emission model in the study of a Schottky barrier of Ni on p- Ga N from current-voltage measurements[J]. *Appl. Phys. Lett.*, 2005, **86**(12):1417.

[13] Roul B, Rajpalke M K, Bhat T N, *et al.* Experimental evidence of Ga-vacancy induced room temperature ferromagnetic behavior in GaN films[J]. *Appl. Phys. Lett.*, 2011, **99**(16):760.

[14] Kenney C, Saraswat K C, Taylor B, et al. Thermionic Field Emission Explanation for Nonlinear Richardson Plots[J]. *IEEE Transactions on Electron Devices*, 2011, **58**(8):2423-2429.

[15] Cheung S K, Cheung N W. Schottky barrier degradation of the W/GaAs system after high - temperature annealing[J]. *J. Appl. Phys.*, 1986, **60**(9):3235-3242.

[16] Suvorova N A, Shchularev A V, Usov I O, *et al.* XPS study of dependence of Au/6H-SiC Schottky barrier height on carrier concentration[J]. *Semiconducting and Insulating Materials, Proceedings of the 10 th Conference*, 1998, 291-294.

[17] Pan S H, Shen H, Hang Z, *et al.* Photoreflectance study of narrow-well strained-layer InGaAs/GaAs coupled multiple-quantum-well structures[J]. *Phys. Rev. B*, 1988, **38**:3375.

[18] Liu J, Mandal K C, Koley G. Investigation of nanoscale electronic properties of CdZnTe crystals by scanning spreading resistance microscopy[J]. *Semicond. Sci. Technol.*, 2009, **24**(4):045012.

[19] Padovani F A, Stratton R. Field and thermionic-field emission in Schottky barriers[J]. *Solid-State Electron*, 1966, **9**(7):695-707.

[20] Hudait M K, Krupanidhi S B. Doping dependence of the barrier height and ideality factor of Au/n-GaAs Schottky diodes at low temperatures [J]. *Physica B*, 2001, **307**(1):125-137.

[21] Pipinys P, Lapeika V. Analysis of reverse-Bias leakage current mechanisms in metal/GaN Schottky diodes[J]. *Advances in Condensed Matter Physics*, 2010, 2010(1687-8108):211-232.

[22] Crofton J, Sriram S. Reverse leakage current calculations for SiC Schottky contacts[J]. *IEEE Transactions on Electron Devices*, 1966, **43**(12):2305-2307.

[23] Stratton R. Theory of field emission from semiconductors[J]. *Phys. Rev.*, 1932, **125**(1):67-82.

[24] Stratton R. Volt-current characteristics for tunneling through insulating films[J]. *J. Phys. Chem. Solids*, 1962, **23**(9):1177-1190.

[25] Suman D, Shen S, Kenneth P R, *et al.* Simulation and design of InAlAs/InGaAs pnp heterojunction bipolar transistors[J]. *IEEE Transactions on Electron Devices*, 1998, **45**(8):1634-1643.

[26] Tan S O, Tecimer H U, Çiçek O, *et al.* Electrical characterizations of Au/ZnO/n-GaAs Schottky diodes under distinct illumination intensities[J]. *J. Mater. Sci-Mater. El.*, 2016, **27**(8):1-8.

[27] Sze S M, Crowell C R, Kahng D. Photoelectric determination of the image force dielectric constant for hot electrons in Schottky barriers [J]. *J. Appl. Phys.*, 1964, **35**(8):2534-2536.